Computation of turbulent flow in a rotating pipe using the structure-based model

By S. V. Poroseva, S. C. Kassinos, C. A. Langer AND W. C. Reynolds

1. Motivation and objectives

Mean rotation induces dynamical effects on turbulence that enter the transport equations through the non-local pressure-strain-rate correlation. It was shown in Kassinos & Reynolds (1994) and Reynolds & Kassinos (1995) that, to describe this effect accurately using one-point turbulence statistics, a turbulence model should include the transport equations not only for Reynolds stresses, but also for additional tensors providing information on turbulence structure missing from the Reynolds stresses. Two second-rank tensors, *dimensionality* D_{ij} and *circulicity* F_{ij}, as well as the third-rank *stropholysis* tensor Q^*_{ijk} along with the Reynolds stresses R_{ij}, form a minimal set of independent tensors necessary for a one-point closure in the case of inhomogeneous turbulence. Relying on these ideas, the structure-based model has been developed in Kassinos & Reynolds (1994-1998) and tested successfully for a wide range of deformations of homogeneous turbulence as well as for some simple wall-bounded flows (Kassinos *et al.*, 2000).

Currently, the structure-based model is being used for the computation of complex inhomogeneous turbulent flows with imposed system rotation. Here we report on the case of a turbulent flow in an axially rotating pipe. Despite the simple geometry, the structure of the turbulence in a rotating pipe flow changes substantially both as the flow develops with downstream distance from the pipe entrance and with increasing rotation rate, and as a result this flow serves as a severe benchmark for any turbulence closure. From a practical point of view, the modeling of a turbulent pipe flow is of interest because it relates to phenomena encountered in various engineering systems involving boundary layers on rotating surfaces, *e.g.*, heat exchangers and rotor cooling systems.

2. Model outline

Information carried by the turbulence structure tensors and the Reynolds stresses can be obtained from a single third-rank tensor $\mathbf{Q}$ (Kassinos & Reynolds, 1994; Reynolds & Kassinos, 1995), which relates to the other structure tensors as:

$$Q^*_{ijk} = \frac{1}{6}\left[Q_{ijk} + Q_{jki} + Q_{kij} + Q_{ikj} + Q_{jik} + Q_{kji}\right],$$

$$R_{ij} = \epsilon_{imp} Q_{mjp}, \quad D_{ij} = \epsilon_{imp} Q_{pmj}, \quad F_{ij} = \epsilon_{imp} Q_{jpm}. \tag{2.1}$$

Therefore, the structure-based model considered in this work includes a model transport equation for the one-point third-rank tensor $\mathbf{Q}$ as well as the standard transport equations for the mean velocity components

$$U_{i,i} = 0, \quad \frac{\bar{D}U_i}{Dt} = \nu U_{i,jj} - < u_i u_j >_{,j} - \tilde{P}_{,i}/\rho, \tag{2.2}$$

and the standard model equation for the dissipation rate ε with a rotation modification (last term) to account for the suppression of ε due to mean rotation (Kassinos *et al.*, 2000):

$$\frac{\bar{D}\varepsilon}{Dt} = \left[\left(\nu\delta_{jk} + \frac{C_\nu}{\sigma_\varepsilon}T < u_j u_k >\right)\varepsilon_{,j}\right]_{,k} - \frac{1}{T}\left(C_o\varepsilon - C_s P\right) - C_\Omega\varepsilon\sqrt{\Omega_j\Omega_k d_{jk}}, \qquad (2.3)$$

where

$$\frac{\bar{D}}{Dt} = U_j\frac{\partial}{\partial x_j} + \frac{\partial}{\partial t}.$$

The equations were derived in the generalized coordinates, but for the sake of simplicity of presentation, the Cartesian tensor notation is used in (2.2)-(2.3) and in what follows. U_i and u_i are components of the mean and fluctuating velocities, $\tilde{P}$ is the mean pressure, ρ is the flow density, ν is the kinematic viscosity, δ_{ij} is the Kronecker delta tensor, ϵ_{ijk} is the Levi-Civita alternating tensor, $q^2 = 2k =< u_i u_i >$ is the turbulent kinetic energy, $< u_i u_j >= R_{ij}$, $P = -R_{ij}U_{i,j}$, $d_{ij} = D_{ij}/q^2$, $\Omega_i = \epsilon_{ijk}U_{k,j}$ is the mean vorticity vector, C_α and σ_β are model coefficients. Time scale T is modeled as $T = \sqrt{(k/\varepsilon)^2 + 36\cdot\nu/\varepsilon}$ (Durbin, 1993).

Now, let us consider the transport equation for **Q**-tensor. In homogeneous turbulence, the transport equation for the **Q**-tensor is (Kassinos *et al.*, 2000):

$$\begin{aligned}\frac{\bar{D}Q_{ijk}}{Dt} = &-G^{(v)}_{jm}Q_{imk} - G^{(n)}_{mk}Q_{ijm} - G^{(v)}_{sm}\epsilon_{its}M_{jmtk} - G^{(n)}_{mt}\epsilon_{its}M_{jsmk} + \\ &(G^{(v)}_{ms} + G^{(n)}_{ms})Q_{ismjk} + 2G^{(n)}_{ms}Q_{ijkms} - \frac{C_1}{\tau^*}\Omega^* f_{ms}(Q_{ijkms} + Q_{jikms}) \\ &-\sqrt{\frac{S_{pq}S_{qp}\Omega_m\Omega_s d_{ms}}{S_{pq}S_{qp} + \Omega_m\Omega_s d_{ms}}}(C_2\epsilon_{ijm}(R_{mk} - D_{mk}) + C_3\epsilon_{ikm}(F_{mj} - D_{mj})) \\ &-C_4\sqrt{\Omega_m\Omega_s d_{ms}}Q^{(R)}_{ijk};\end{aligned} \qquad (2.4)$$

$$Q^{(R)}_{ijk} = Q_{ijk} - \frac{1}{6}(-\epsilon_{ijk}q^2 - \epsilon_{ikm}D_{mj} + 2\epsilon_{jim}D_{mk} - \epsilon_{kjm}D_{mi}), \quad G_{ij} = U_{i,j}.$$

C_1, C_2, C_3, and C_4 are model coefficients, which are chosen to be equal to 8.5, 0.2, 0.1, and 0.5 respectively. The detailed explanation of Eq. (2.4) is given in Kassinos & Reynolds (1998) and Kassinos *et al.* (2000). Here, we just note that the fourth-rank tensor **M** can be obtained from Q_{ijkmn} by contracting with ϵ_{ijk}, and for weak anisotropies Q_{ijkmn} can be modeled as a linear function of Q_{ijk} (Kassinos *et al.*, 2000).

To take into account inhomogeneous effects such as turbulent transport and the influence of the wall on the turbulence structure, some modifications to (2.4) have been suggested by Kassinos *et al.* (2000). Turbulent and molecular transport is incorporated in Eq. (2.4) through the additional model term:

$$\Gamma_{ijk} = \left[\left(\nu\delta_{mn} + \frac{C_\nu}{\sigma_Q}T < u_m u_n >\right)Q_{ijk,m}\right]_{,n}. \qquad (2.5)$$

Model (2.5) is derived in such a way that after contraction with ϵ_{lik} it gives the known model presentation of the turbulent diffusion term (Daly & Harlow, 1970) in the transport

equation for R_{lj}:

$$\Gamma_{lj} = \epsilon_{lik}\Gamma_{ijk} = \left[\left(\nu\delta_{mn} + \frac{C_\nu}{\sigma_Q}T < u_m u_n >\right) R_{lj,m}\right]_{,n}.$$

Near-wall effects are incorporated in the **Q**-equation through an elliptic relaxation scheme based on ideas of Durbin (1993). If $\wp_{ijk}$ denotes the right-hand side of (2.4), then, all terms in $\wp_{ijk}$ that are not associated with either production or dissipation of the turbulent kinetic energy are lumped in a term named Π_{ijk}. The simplest model for Π_{ijk} is

$$\Pi_{ijk} = \wp_{ijk} - H_{ijk}, \tag{2.6}$$

where

$$H_{ijk} = -G_{jm}Q_{imk} - \frac{1}{2}G_{tm}\epsilon_{tik}R_{mj} + \frac{1}{2}(Q_{imk} + Q_{kmi}) - \frac{1}{T}Q_{ijk}$$

(Kassinos *et al.*, 2000).

Expression (2.6) is a model for redistributive processes that is valid for homogeneous turbulence. Now, we use kf_{ijk} to denote an augmented version of this model that is valid in inhomogeneous turbulence. The components of the tensorial function f_{ijk} are found from the elliptic relaxation equation:

$$L^2\nabla^2 f_{ijk} - f_{ijk} = -\frac{\Pi_{ijk}}{k}. \tag{2.7}$$

With models (2.5) - (2.7), governing Eq. (2.4) for Q_{ijk} in an inhomogeneous flow takes the form:

$$\frac{DQ_{ijk}}{Dt} = \left[\left(\nu\delta_{mn} + \frac{C_\nu}{\sigma_Q}T < u_m u_n >\right) Q_{ijk,m}\right]_{,n} + kf_{ijk} + H_{ijk}.$$

3. Numerical procedure

To compute a pipe flow, all equations were written using the boundary layer approximation in the axisymmetric cylindrical frame of reference $x^i = (x, r, \varphi)$, where x, r, and φ are axial, radial, and angular coordinates respectively. In such coordinates, the covariant and contravariant components of the velocity are $U_i = (U, V, rW)$, $U^i = (U, V, W/r)$. The control volume technique (Spalding, 1977) was used to solve the transport equations.

In the computation we used the same conditions as those in the experiments of Zaets, Safarov & Safarov (1985), where a swirling flow was obtained by conveying a fully-developed turbulent flow ($U_o = 10^3$ cm/sec, $\nu = 0.149$ cm^2/sec, friction velocity $u_{*o} =$ 43.5 cm/sec) from a stationary straight cylindrical pipe of 100-diameter length into a rotating cylindrical section of the same diameter ($D = 6$ cm).

On the pipe axis the boundary conditions are:

$$\frac{\partial U}{\partial r} = \frac{\partial \varepsilon}{\partial r} = W = 0, \quad U = U_o, \quad \frac{\partial Q_{ijk}}{\partial r} = 0 \quad \text{if} \quad i = j, \quad \text{or} \quad j = k, \quad \text{or} \quad i = k,$$

$$\text{and} \quad Q_{ijk} = 0, \quad \text{if} \quad i \neq j \neq k.$$

At the wall,

$$U = Q_{ijk} = 0, \quad W = W_o, \quad \varepsilon_w = \frac{2\nu k_w}{y_w^2},$$

where k_w is the value of the turbulent kinetic energy at the last grid node next to the

wall and y_w is the distance between the wall and that node. This last condition ensures that $k_w = O(y_w^2)$.

The correct behavior of the different components of the **Q**-tensor was obtained by applying appropriate boundary conditions on f_{ijk}. The limiting behavior for each Q_{ijk}-component was derived by Kassinos (private communication). In particular, he showed that the correct behavior of Q_{ijk} components should give the correct behavior of the corresponding Reynolds stresses (Eq. (2.1)). Following these principles, the boundary conditions for f_{ijk} were derived and verified by comparison with DNS data (Moser, Kim & Mansour, 1988) by Langer (private communication) for a channel flow. Comparison of the DNS data for a channel (Moser, Kim & Mansour, 1988) and for a pipe (Eggels *et al.*, 1994) shows that in the near-wall area turbulent statistics behave in the same way in both flows. Therefore, in the present work, similar boundary conditions were applied to f_{ijk} at the pipe wall:

$$f^{(w)}_{xx\varphi} = -\frac{20\nu^2 Q_{xx\varphi}}{\varepsilon_w y_w^4}, \quad f^{(w)}_{\varphi\varphi x} = -\frac{20\nu^2 Q_{\varphi\varphi x}}{\varepsilon_w y_w^4}, \quad f^{(w)}_{x\varphi\varphi} = -\frac{20\nu^2 Q_{x\varphi\varphi}}{\varepsilon_w y_w^4},$$

$$f^{(w)}_{\varphi x x} = -\frac{20\nu^2 Q_{\varphi x x}}{\varepsilon_w y_w^4}, \quad f^{(w)}_{\varphi r x} = -\frac{20\nu^2 Q_{\varphi r x}}{\varepsilon_w y_w^4}, \quad f^{(w)}_{x r\varphi} = -\frac{20\nu^2 Q_{x r\varphi}}{\varepsilon_w y_w^4},$$

$$f^{(w)}_{xii} = 0, \; f^{(w)}_{iix} = 0, \quad f^{(w)}_{\varphi ii} = 0, \; f^{(w)}_{ii\varphi} = 0,$$

$$f^{(w)}_{\alpha\alpha\alpha} = 0 \quad \text{(no summation over } \alpha);$$

$$f^{(w)}_{r\phi x} = -0.2 f^{(w)}_{xr\varphi} = 0, \quad f^{(w)}_{\phi x r} = -0.8 f^{(w)}_{xr\varphi} = 0,$$

$$f^{(w)}_{x\phi r} = -0.2 f^{(w)}_{\varphi r x} = 0, \quad f^{(w)}_{rx\phi xr} = -0.8 f^{(w)}_{\varphi r x} = 0.$$

The rest of the components are equal to zero at the wall. On the pipe axis, the boundary conditions for f_{ijk} are the same as for Q_{ijk}.

Equation (2.7) was solved using a standard finite-difference scheme. The grid was non-uniform in r, with the total number of N nodes being 64 for $Re_o = U_o D/\nu = 4 \cdot 10^4$ and 81 for $Re_o = 7 \cdot 10^3$ (D is the pipe diameter, $R = D/2$). The streamwise grid spacing δx was $0.0001R$.

For the length scale L in (2.7), various functional forms, including the ones suggested in Durbin (1993) and Pettersson, Andersson & Brunvoll (1998), have been tested. However, it was found that the best results were obtained by using a simple function like $L^2 = 1$, at $y_+ \leq 60$, and $L^2 = 0$, at $y_+ \geq 60$. Despite its simplicity this form seems somewhat unphysical, and even though here we are reporting results based on this form of L, we are currently pursuing a more fundamental basis for the length scale profile. It is also worth noting that in the initial section of the rotating pipe, where strong suppression of turbulence statistics occurs in the whole flow area including the near-wall one, the influence of this length scale is rather weak. At a rotation number of $N = W_o/U_o = 0.6$, both the peak value as well as the extent of the profile of L from the pipe wall seem to have practically no influence on the results of the calculations.

4. Results

As experiments demonstrate, it is possible to distinguish two regions in a rotating pipe flow with different turbulence structure: the initial section of a pipe with the length of

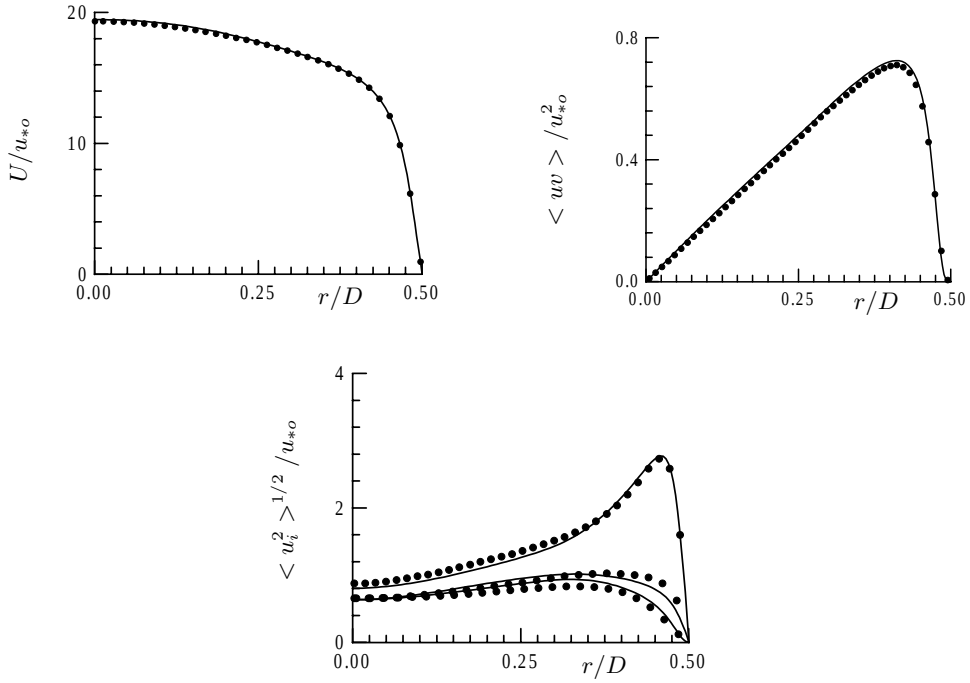

FIGURE 1. Stationary pipe flow: (———) **Q**-model, (●) DNS data.

about $30D$ and the fully developed turbulent flow which is observed at about $170D$. In the former region, strong turbulence suppression is observed (Zaets, Safarov & Safarov, 1985). In the latter one, profiles of statistical variables reach their limit shapes (Kikuyama *et al.*, 1983; Nishibori, Kikuyama & Murakami, 1987; Imao, Itoh & Harada, 1996, in particular).

The components of the mean velocity behave monotonically along the pipe axis and under rotation. The profile of the axial component tends to be parabolic as the one in a laminar flow, but does not reach this shape. The profile of the angular component has nearly parabolic limit shape ($W/W_o = (r/R)^2$, R is the pipe radius) instead of the expected linear one as it would be in the case of a forced rotational flow.

In contrast to the mean velocity components, the velocity moments of second and higher orders behave non-monotonically with increase of one of the parameters: downstream distance from the pipe entrance or rotation number. In the initial pipe section, indeed, strong suppression of turbulence characteristics is observed (Zaets, Safarov & Safarov, 1985). After suppression, however, they increase in the value and are stabilized on the high level enough (Nishibori, Kikuyama & Murakami, 1987).

In the following subsections, the results of computations using the **Q**-model are presented for the various regimes of a turbulent pipe flow.

4.1. *Stationary pipe*

Calculations have been done for a turbulent flow in a stationary pipe at two Reynolds numbers, $Re_o = 7 \cdot 10^3$ and $Re_o = 4 \cdot 10^4$, to verify an ability of the **Q**-model to give reasonable results in both low and high Reynolds number regimes. The results were

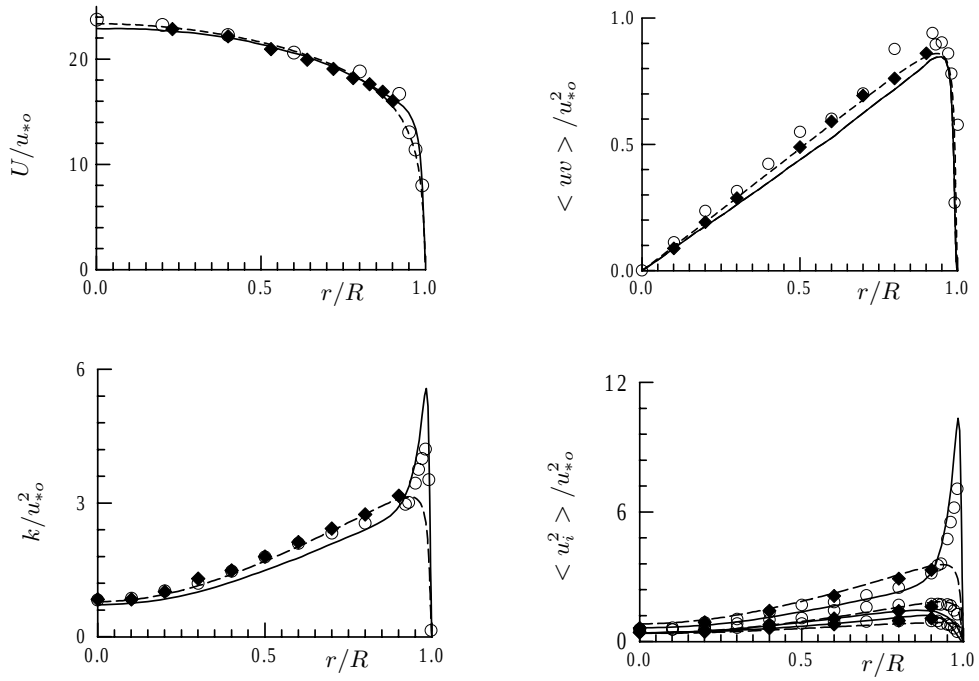

FIGURE 2. Calculations: (———) **Q**-model, (– – – –) RSTM; experiments: (♦) Zaets, Safarov & Safarov (1985), (○) Laufer (1954).

compared for $Re_o = 4{\cdot}10^4$ (Fig. 2) with the experimental data of Zaets, Safarov & Safarov (1985) and Laufer (1954). The latter were obtained at $Re_o = 5 \cdot 10^4$. For $Re_o = 7 \cdot 10^3$ (Fig. 1), the DNS data (Eggels *et al.*, 1994) were used for comparison. As shown in Figs. 1 and 2, the model gives quite good results.

In Fig. 2, profiles are also shown from the calculations of Kurbatskii, Poroseva & Yakovenko (1995) that used the linear Reynolds stress transport (RST) model (IP model (Launder, Reece & Rodi, 1975) with the damping functions similar to ones suggested in Gibson & Launder (1978) to describe wall effects). Though this model reproduces turbulent characteristics and mean velocity well enough at the high Reynolds number, it describes only qualitatively the features of the low Reynolds number flow.

To describe flows at different Reynolds numbers, the coefficient C_s in Eq. (2.3) varies from 1.58 at $Re_o = 4 \cdot 10^4$ to 1.65 at $Re_o = 7 \cdot 10^3$. In both cases this value differs from the value found optimal for a homogeneous flow; that is, $C_s = 1.5$. The similar situation is observed when the RST models are used. The other model coefficients are found to be $\sigma_Q = 1,\ \sigma_\varepsilon = 1.1,\ C_\nu = 0.22$.

4.2. *Initial section of a rotating pipe*

It was found that to describe the strong suppression of the turbulence observed in this part of the flow, one has to modify the equation for the dissipation rate by including the additional term with the Richardson number (Kurbatskii, Poroseva & Yakovenko, 1995). The Richardson number characterizes the influence of streamline curvature on turbulence like that of medium stratification on turbulent transport (Bradshaw, 1969). The same modification was introduced in ε-equation (2.3) used with the **Q**-model; that

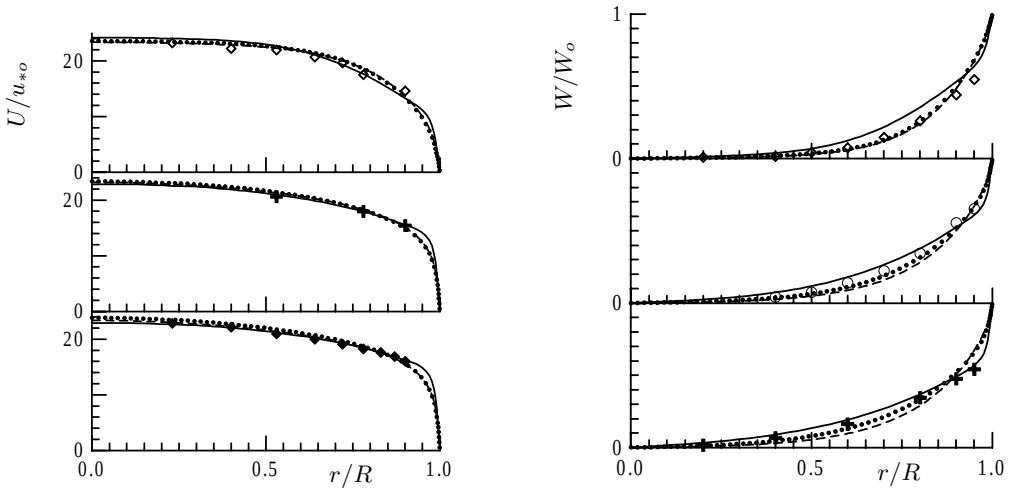

FIGURE 3. Mean velocity components. Calculations:(———) **Q**-model, (– – – –) IP, (·····) SSG1; (♦) $N = 0.$, (+) $N = 0.15$, (○) $N = 0.3$, (◊) $N = 0.6$.

is, the coefficient C_o was changed by C_o^*, where

$$C_o^* = \max(1.4, C_o(1 - C_R Ri)), \quad C_R = 2, \quad C_o = 11/6, \quad Ri = \frac{\frac{\partial W}{\partial r} \cdot \frac{W}{r}}{\left(\frac{\partial W}{\partial r}\right)^2 + \left(\frac{\partial U}{\partial r}\right)^2}$$

The condition on C_o^* is applied to avoid excessive values of the dissipation rate close to a wall, which can occur under rotation.

The turbulent flow in the initial pipe section ($x/D \leq 25$) was computed at $Re_o = 4{\cdot}10^4$. In Figs. 3-6 the calculated profiles are compared with the experimental data (Zaets, Safarov & Safarov, 1985) and with the results of calculation by RST models: linear (IP) and non-linear (SSG1) (Speziale, Younis & Berger, 2000). In both RST models, damping functions similar to the ones suggested in Gibson & Launder (1978) were applied to describe wall effects. Profiles in Figs. 3-5 correspond to the section $x/D = 25$. As shown, the **Q**-model describes quite well the axial velocity profiles in the whole flow area: from the wall to the pipe axis at different rotation numbers. Moreover, the **Q**-model catches correctly dynamics of the axial velocity with increasing rotation. That is, at the low rotation number $N = 0.15$, the axis value of U slightly decreases, but with further increasing of N, it begins to grow. The behavior of the angular component of the mean flow velocity also is well reproduced.

The behavior of turbulent statistics is reproduced very well, especially near the pipe axis (Figs. 4-6). This is an important result because turbulent transport at the core of a pipe flow at moderate swirl is similar to turbulent transport in concentrated vortex formations in the atmosphere. The damping coefficient Ku_i on Figs. 5-6 is determined as $Ku_i = < u_i^2 > (N > 0) / < u_i^2 > (N = 0)$.

In experiments it has been observed that near the pipe entrance there exists a conical core in which the developing turbulence is only weakly influenced by the rotation. The streamwise extent of this conical core decreases with increasing rotation. The **Q**-model is more sensitive to the influence of rotation on this initial pipe section and describes

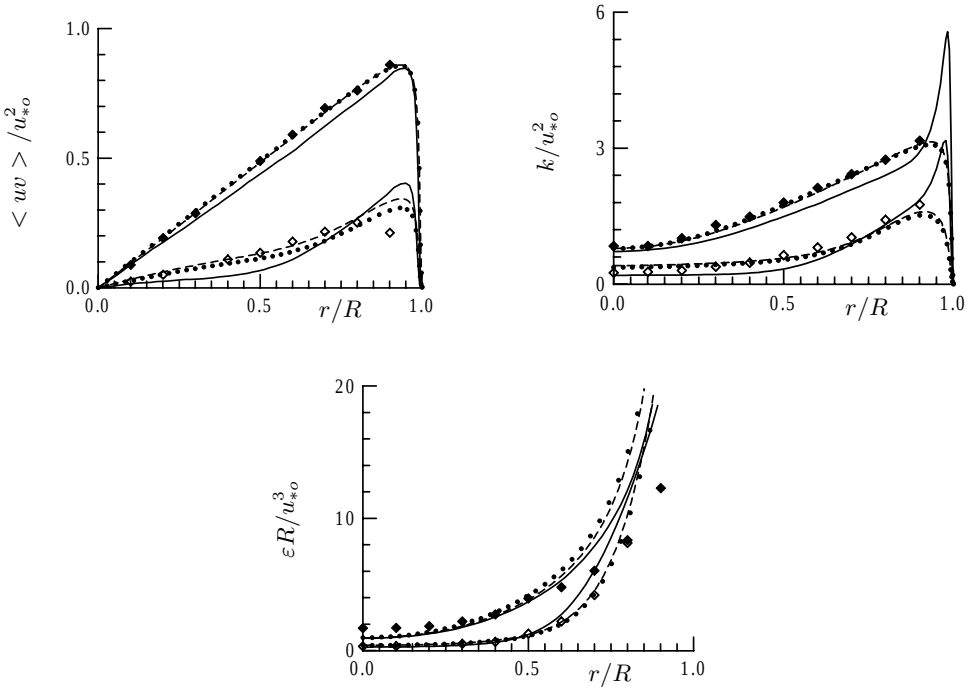

FIGURE 4. (See denotations on Fig. 3).

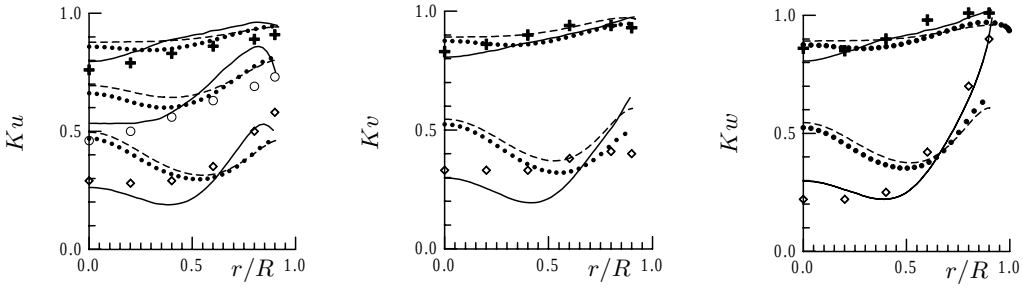

FIGURE 5. (See denotations on Fig. 3.)

correctly the shortening of the conical core. In contrast, the RST model is less sensitive to rotational effects in this section and tends to overpredict the extent of the conical core (especially near the centerline) as the rotation is increased. This effect is shown in Fig. 6 where the streamwise evolution of Ku is shown along the initial pipe section.

Finally, it is worth noting that in the initial pipe section, the performance of linear and non-linear RST models are comparable.

4.3. *Fully developed flow*

With increasing rotation and distance from the pipe entrance, the **Q**-model with ε-equation (2.3) using the modified C_o^* predicts full suppression of the turbulence, like the RST models do, in contradiction with the experimental data. Therefore, a fully de-

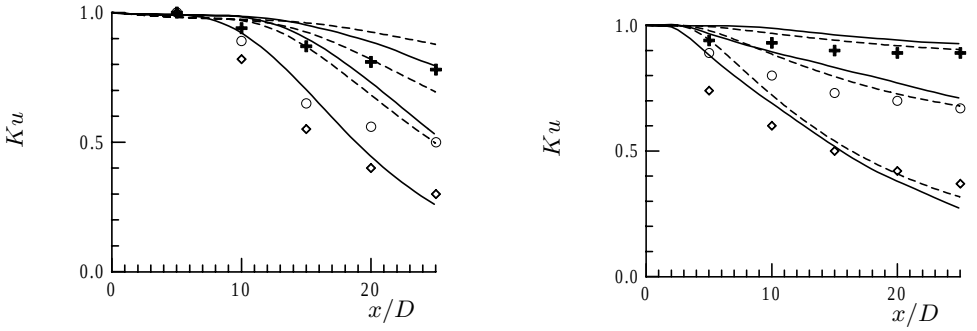

$r/R = 0.$ $r/R = 0.6$

FIGURE 6. Evolution of Ku along the pipe axis. (See denotations on Fig. 3.)

veloped turbulent flow in a rotating pipe was computed by the **Q**-model with ε-equation (2.3) without modification by C_o^*. Some results obtained at $Re_o = 2 \cdot 10^4$ are shown on Fig. 7 in comparison with the experimental data of Imao, Itoh & Harada (1996) and the data obtained with the non-linear RST model (SSG2) (Speziale, Younis & Berger, 2000) with a near-wall model developed in Durbin (1993).

The flow simulated by the **Q**-model reaches the fully developed state at the distance close to the experimental value (Kikuyama *et al.*, 1983; Nishibori, Kikuyama & Murakami, 1987). The model reproduces the evolution of the axial component of the mean velocity better than the RST models do. For the angular velocity, the computational results obtained with the **Q**-model are close to the profiles obtained with the linear RST models (Pettersson, Andersson & Brunvoll, 1998; Speziale, Younis & Berger, 2000; Kurbatskii & Poroseva, 1999). The non-linear RST model provides better agreement for W with the experimental data.

The shear stresses are reproduced well with the **Q**-model. However, in this part of the flow, like other turbulence models, the **Q**-model significantly overpredicts the turbulent kinetic energy level in comparison with experimental data.

Most importantly, the **Q**-model is able to reproduce the correct behavior of turbulence characteristics at relatively high rotation rates, *e.g.*, $N = 1$, whereas RST models predict relaminarization of the flow (Pettersson, Andersson & Brunvoll, 1998) already at this N in contrast to the experiments of Kikuyama *et al.* (1983), which show no sign of turbulence disappearance even at considerably higher N.

5. Conclusions and future plans

The main goal of the present work was to test the **Q**-model in a complex rotated turbulent flow and compare its performance with that of RST models, using in all models similar equations for the dissipation rate.

The **Q**-model is able to predict the flow accurately at various Reynolds numbers and under stronger rotation than possible with a good RST model. In the fully developed pipe flow at moderate rotation numbers, the **Q**-model slightly improves the profiles obtained with the non-linear RST model, which gives the best results among RST models for this part of flow. Most importantly, the **Q**-model is able to reproduce the correct behavior of turbulence characteristics at relatively high rotation rates, *e.g.*, $N = 1$, whereas the RST models predict relaminarization of the flow in contrast to experiments. Also, under

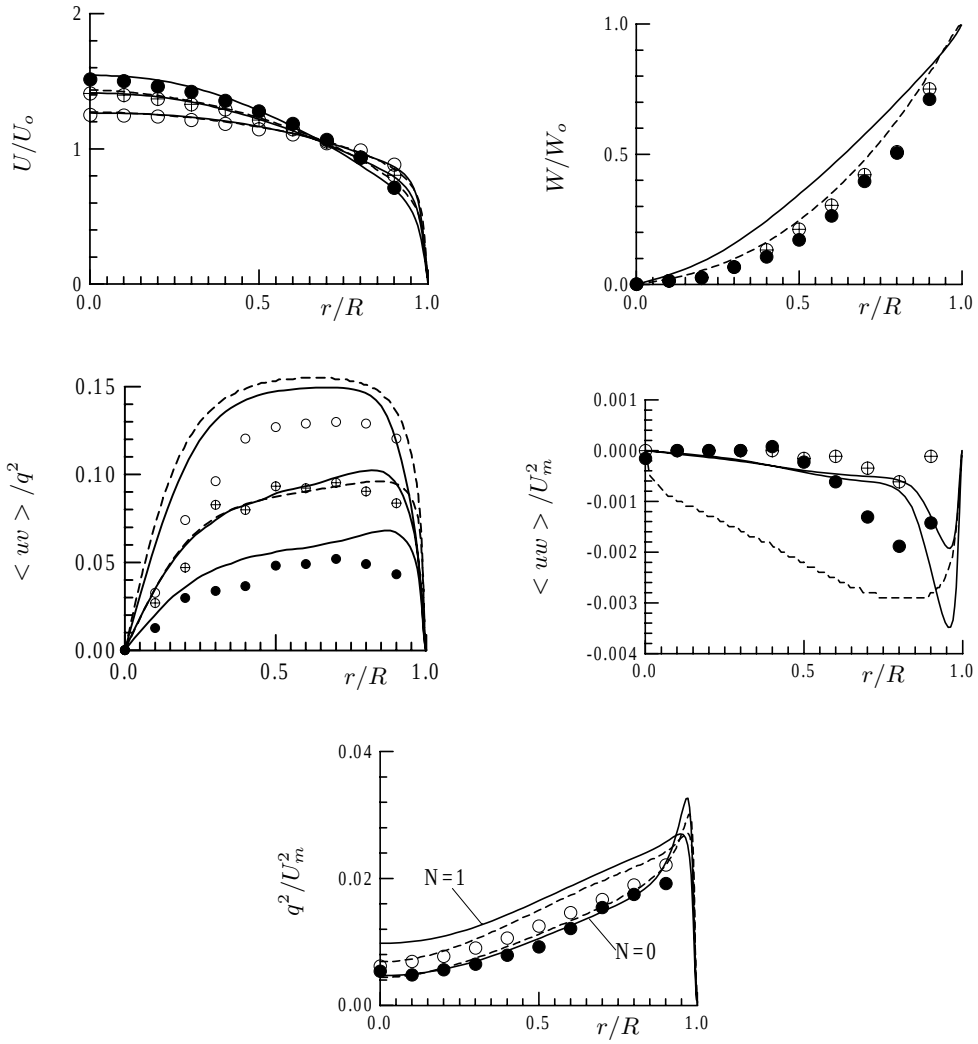

FIGURE 7. Fully developed pipe flow. Calculations:(———) **Q**-model, (– – – –) SSG2; experiments: (○) $N = 0.$, (⊕) $N = 0.5$, (●) $N = 1$.

some parameter combinations (N, Re) computations using RST models fail to converge (Pettersson, Andersson & Brunvoll, 1998; Kurbatskii & Poroseva, 1999), whereas such difficulties have not been encountered with the **Q**-model.

However, the **Q**-model as tested in this work, does not solve all problems. One of the possible reasons for this is that, in order to be consistent, a one-point turbulence closure based on the transport equation for Q should also include structure information in the equation for the dissipation rate ε. We are currently working in this direction and hope to be able to report on our progress soon. In the RST models, such modifications would not be possible since they do not carry the necessary information. We are also working on improving the length scale model used in the elliptic relaxation of Q. Finally, we

are currently using these ideas as the basis for the development of a simplified algebraic two-equation structure-based model.

Acknowledgments

We would like to thank Dr. B. A. Pettersson-Reif for providing the simulation data obtained with the non-linear SSG2 model in the fully developed pipe flow (Figs. 7).

REFERENCES

Bradshaw, P. 1969 The analogy between streamline curvature and buoyancy in turbulent shear flow. *J. Fluid Mech.* **36**, 177-191.

Daly, B. J. & Harlow, F. H. 1970 Transport equations in turbulence. *Phys. Fluids.* **13**(11), 2634-2649.

Durbin, P. 1993 A Reynolds-stress model for near-wall turbulence. *J. Fluid Mech.* **249**, 465-498.

Eggels, J. G. M., Unger, F., Weiss, M. H., Westerweel, J., Adrian, R. J., Friedrich, R. & Nieuwstadt, F. T. M. 1994 Fully developed turbulent pipe flow: a comparison between direct numerical simulation and experiment. *J. Fluid Mech.* **268**, 175-209.

Gibson, M. M. & Launder, B. E. 1978 Ground effects on pressure fluctuations in the atmospheric boundary layer. *J. Fluid Mech.* **86**, 491-511.

Imao, S., Itoh, M. & Harada, T. 1996 Turbulent characteristics of the flow in an axially rotating pipe. *Int. J. Heat and Fluid Flow* **17**(5), 444-451.

Kassinos, S. C. & Reynolds, W. C. 1994 A structure - based model for the rapid distortion of homogeneous turbulence. *Report TF - 61,* Thermosciences Division, Department of Mechanical Engineering, Stanford University.

Kassinos, S. C. & Reynolds, W. C. 1995 An extended structure - based model based on a stochastic eddy - axis evolution equation. it Annual Research Briefs, Center for Turbulence Research, NASA Ames/Stanford University. 133-148.

Kassinos, S. C. & Reynolds, W. C. 1996 An interacting particle representation model for the deformation of homogeneous turbulence. *Annual Research Briefs,* Center for Turbulence Research, NASA Ames/Stanford University. 31-53.

Kassinos, S. C. & Reynolds, W. C. 1997 Advances in structure - based modeling. *Annual Research Briefs,* Center for Turbulence Research, NASA Ames/Stanford University. 179-193.

Kassinos, S. C. & Reynolds, W. C. 1998 A structure - based model with strophol-ysis effects. *Annual Research Briefs,* Center for Turbulence Research, NASA Ames/Stanford University. 197-209.

Kassinos, S. C., Langer, C. A., Haire, S. L. & Reynolds, W. C. 2000 Structure - based turbulence modeling for wall-bounded flows. *Int. J. Heat and Fluid Flow.* **21**, 599-605.

Kikuyama, K. *et al.* 1983 Flow in an axially rotating pipe (a calculation of flow in the saturated region). *Bull. JSME.* **26**(214), 506-513.

Kurbatskii, A. F., Poroseva, S. V. & Yakovenko, S. N. 1995 Calculation of statistical characteristics of a turbulent flow in a rotated cylindrical pipe. *High Temperature.* **133** (5), 738-748.

Kurbatskii, A. F. & Poroseva, S. V. 1999 Modelling turbulent diffusion in a rotating cylindrical pipe flow. *Int. J. Heat and Fluid Flow.* **20**(3), 341-348.

Laufer, J. 1954 The structure of turbulence in fully developed pipe flow. *NASA Report N 1174.*

Launder, B. E., Reece, G. J. & Rodi, W. 1975 Progress in development of a Reynolds-stress turbulent closure. *J. Fluid Mech.* **68**, 537-566.

Moser, R. D., Kim, J. & Mansour, N. N. 1988 Direct numerical simulation of turbulent channel flow up to $Re_\tau = 590$. *Phys. Fluids.* **11**(4), 943-945.

Nishibori, K., Kikuyama, K., & Murakami M. 1987 Laminarization of turbulent flow in the inlet region of an axially rotating pipe. *Bull. JSME.* **30**(260), 255-262.

Pettersson, B. A., Andersson, H. I. & Brunvoll, A. S. 1998 Modeling near - wall effects in axially rotating pipe flow by elliptic relaxation. *AIAA J.* **36**(7), 1164-1170.

Reynolds, W. C. & Kassinos, S. C. 1995 A one - point model for the evolution of the Reynolds stress and structure tensors in rapidly deformed homogeneous turbulence. *Proceed. Roy. Soc. London A.* **451** (1941), 87-104.

Spalding, D. B. 1977 *GENMIX: a General Computer Program for Two - Dimensional Parabolic Phenomena.* Pergamon Press.

Speziale, C.G., Younis, B. A. & Berger, S. A. 2000 Analysis and modeling of turbulent flow in an axially rotating pipe. *J. Fluid Mech.* **407**, 1-26.

Zaets, P. G., Safarov, N. A., & Safarov R.A. 1985 Experimental study of the behavior of turbulence characteristics in a pipe rotating around its axis (in Russian). *Modern problems of continuous medium mechanics*, Moscow Physics and Technics Institute. 136-142.